Proceedings of the 2022 Design of Medical Devices Conference
DMD2022
April 11-14, 2022, Minneapolis, MN, USA

DMD2022-1042

ADDITIVE MANUFACTURING OF MEDICAL MICRODEVICES

Renc Saracaydin
Mayo Clinic
Rochester, Minnesota, USA

Seth A. Hara
Mayo Clinic
Rochester, Minnesota, USA

ABSTRACT

Additive manufacturing is a growing field, but its application in the fabrication of medical microdevices has not been fully explored. Traditionally, medical microdevices are manufactured via a combination of techniques such as photolithography, laser-cutting, and micromolding, which collectively have challenges such as multiple fabrication steps, limited design freedom, high fabrication cost, and significant fabrication time. Micro vat photopolymerization is presented here as an alternative method to produce four different microscale medical devices that have applications in microfluidics, drug delivery, and bioscaffolding. In terms of minimum feature size and resolution, the presented structures are comparable, if not superior, to literature quoted parts fabricated through conventional manufacturing methods. The fabrication steps, process parameters, design considerations, learnings, and future research directions are outlined.

Keywords: Additive manufacturing, medical microdevices, microfluidics, drug delivery systems, bioscaffolds.

1. INTRODUCTION

Additive manufacturing, also known as 3D printing, is a fabrication method in which parts are printed layer by layer. Recently, it has been experiencing a great deal of interest in various industries such as automotive, aerospace, electronics, construction, and medical which is the focus of this paper [1]. In the biomedical sector, additive manufacturing of surgical cutting guides, anatomic models, and prosthetics are already being adopted [2]. Additionally, its application in regenerative medicine, patient specific implants, and bioprinting are burgeoning [2]. However, its presence in the fabrication of microscale medical devices such as microfluidics, drug delivery systems, and BioMEMS is just beginning to be explored.

Conventionally, the fabrication of medical devices with micrometer sized features is carried out by a combination of techniques such as lithography, laser-cutting, and micromolding [3]. Although these techniques are well established and can provide devices with high quality, they have their own challenges and drawbacks. They require long process development cycles and multiple fabrication steps, ultimately increasing the manufacturing time and cost. Furthermore, these techniques are not easily applicable to highly iterative design and prototyping processes and have limited design freedom such that some complex three-dimensional architectures are unattainable. Additive manufacturing can address some of these challenges to build structures at a relatively lower cost and shorter time with a greater design freedom compared to conventional methods.

Presented here are four microscale medical devices to demonstrate that micro-additive manufacturing is a viable option for the fabrication of microscale medical devices. Two-dimensional (2D) Tesla valve, microlumen array, microneedle array, and a cubic fluorite microlattice were printed to showcase that micro vat photopolymerization can be used as a fabrication technique for microfluidic, drug delivery, and bioscaffolding applications. The goal of this study was not to prove the function of these devices but instead show that they can be 3D printed with a very high quality that rivals those made using conventional methods. Additionally, the learnings, challenges, and possible directions for future research are outlined to help the scientific community build on the work presented here.

2. MATERIALS AND METHODS

2.1 Fabrication setup

All presented structures were printed on the Kloé Dilase 3D, a microscale vat photopolymerization 3D printer (Fig. 1). It consists of two sections, the bottom part containing a continuous wave (CW) 70 mW laser diode of 375 nm emission wavelength, and the top section composed of a tank and a motorized sample holder. The laser coupled to a 10X objective (Olympus, UPlanFL N 10x/0.30 FN 26.5 UIS 2) ensures a beam diameter of 5µm for

single-photon photopolymerization. All optical elements are mounted on a magnetic stage that has a travel resolution and repeatability of 100 nm in *x* and *y* directions. The writing speed of the laser ranges from 0.001 mm/s to 100 mm/s, while the laser power can be modulated from 0.001% to 100%.

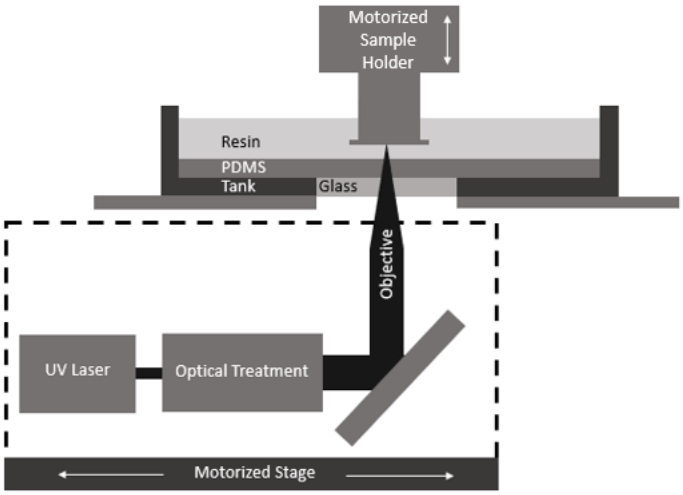

FIGURE 1: Dilase 3D schematic.

The build volume is 10(*x*) x 10(*y*) x 5(*z*) cm^3 and the dimensions of the tank are 10(*x*) x 10(*y*) x 1(*z*) cm^3, allowing large parts to be printed with ultra-fine resolution from a few millimeters of photocrosslinkable resins. The glass window at the bottom of the tank is covered with a polydimethylsiloxane (PDMS) slab of uniform thickness of 2mm to prevent the cured parts from sticking to the tank during the printing process. The sample holder is fixed on a stage that moves in the *z* direction with a resolution of 500nm and repeatability of 1µm. To ensure consistent performance, a slice thickness ranging from 5µm to 10 µm was used in this work.

2.2 Fabrication process

The parts were either designed in SolidWorks or downloaded from Thingiverse, a website providing open-source hardware designs licensed under GNU General Public License or Creative Commons licences. The CAD (computer-aided design) files were saved as .stl files and sliced horizontally by 3DSlicer software (Kloé SA). The sliced files, named .lwo files, were imported into DilaseSoft software (Kloé SA) for printing. These software allow control of all the build parameters that need to be set for each slice and optimized for each structure. These include laser power, velocity, pitch (overlap), writing direction, filling strategy, stabilization length, and delay time between layers. Briefly, the laser power is the percentage of the laser energy that is deposited to the resin, such that a higher power cures the resin more aggressively compared to lower percentages. Laser velocity is the velocity with which the laser scans the resin, such that the level of exposure increases as velocity decreases. The pitch determines the percentage of overlap between two successive laser scans which can be written on either *x* or *y* directions. A large pitch overlap leads to an increased number of scan lines for a given structure, resulting in features with high-definition perpendicular to the writing direction. The filling strategy is used to determine whether patterns on each slice are filled, contoured or both; structures presented here were only filled and not contoured. The stabilization length is the length traveled by the laser before it turns on and starts exposing the pattern, allowing it to reach the set velocity before starting the exposure. Higher laser velocities require longer stabilization lengths so that the laser has adequate time to reach desired velocities. Lastly, a delay time between each layer can be instituted, allowing the resin to diffuse between the cured layer and the PDMS slab and relax. This becomes increasingly important when large or very thin cross-sections are printed.

Once the structures are printed, they are immersed in isopropyl alcohol (Sigma, 190764) to wash away uncured resin, dried with a nitrogen gun, and cured under ultraviolet (UV) light to finalize the photopolymerization reaction [4]. The exact wash and cure profiles depend on the size and geometry of the printed parts. All presented structures were manufactured using a commercial UV-curable resin (DS3000, DWS Systems).

2.3 Designed geometric features of structures

The *two-dimensional (2D) Tesla Valve* has an overall size of 0.85(*x*) x 3.6(*y*) x 0.12(*z*) mm^3 and a channel width and depth of 50(*x* and *z*) µm. The *microneedle array* consists of 25 identical conical shapes with heights, base diameters, and edge-to-edge separations of 650(*z*) µm, 200(*x* and *y*) µm, and 300(*x* and *y*) µm, respectively. The *microlumen array* consists of 4,096 identical lumens with diameters, heights, and edge-to-edge separations of 10(*x* and *y*), 30(*z*), and 20(*x* and *y*) µm, respectively. The *cubic fluorite microlattice* has an overall size of 3.43(*x*) x 3.43(*y*) x 3.43(z) mm^3. The strut diameters are 65 µm and the perforations are 95 µm wide. All structures were printed on the center of400(*z*) µm thick rectangular pedestals that are 1 mm larger in *x* and *y* directions compared to first layers of the printed structures. These serve as bases, ensuring tight adhesion of the printed structures to the sample holder.

2.4 Characterization of printed parts

Printed parts were investigated under digital light and scanning electron microscopes. A Keyence VHX-7000 digital light microscope was used to image and measure the printed structures at magnifications ranging from 40X to 300X. The dimensions of the parts were measured at 10 different locations and averaged for statistical analysis. SEM imaging was performed using a Hitachi S-4700 with acceleration voltages at 0.7kV or 1kV.

3. RESULTS AND DISCUSSION

3.1 Two-dimensional (2D) Tesla Valve

A *two-dimensional (2D) Tesla valve* designed for microfluidic applications was printed. The structure started with a flat pedestal that needed to be properly exposed to serve as a platform on which the part can be built. It was discovered that overexposed bases allowed tight adhesion between the part and the build platform but at the expanse of part quality. On the other hand, underexposed bases did not ensure tight adhesion and the part detached either during the printing process or the washing procedure. Additionally, the bases needed to be relatively thick so that they were structurally rigid to preserve the mechanical stability of the printed parts and enable their safe handling. It was found that 400μm thick bases z-sliced at 50μm/layer and fabricated at 75% laser power and at 20mm/s writing speed met the above-mentioned criteria. These build parameters were used for the bases of all presented parts.

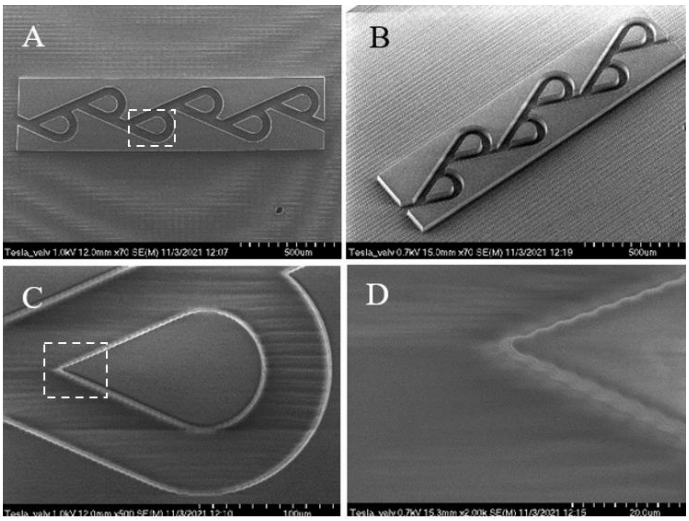

FIGURE 2: Scanning electron micrographs of 2D Tesla valve shown in (A) top view and (B) isometric view. Higher magnifications of the framed regions are shown in C and D.

The valvular conduit (Fig. 2) was fabricated with a slice thickness of 10μm/layer in a little less than 2 hours. After the printing process, the sample was immersed in two subsequent (isopropyl alcohol) IPA baths of 5 minutes each to wash away the uncured resin. It was dried with nitrogen gun after each IPA bath and finally post-cured under UV light for 5 minutes. In terms of process parameters, a low velocity of 3mm/s was chosen because the structure had features as small as 5μm, meaning that the laser needed to turn on and off in a very short distance. This was only possible if the laser was moving slowly; a faster writing speed would have not resolved this level of fine features. Since the writing speed was very low, the stabilization length was also set to a low value of 1mm/s, minimizing the print time. Additionally, a large pitch overlap of 90% was utilized so that the channels and the tear drops in the valvular conduit could be printed with high resolution. This was especially evident on the surfaces that are perpendicular to the writing direction which was along the long edge of the structure. The choice of writing direction was selected such that the tear drops could be printed head on instead of perpendicular to the features, allowing their tips to be printed with ultra-fine resolution. The printed tip was measured to be around 2.5μm which could have not been possible if the laser was moving across the tip. The low velocity and high overlap were counterbalanced with a low modulation of 10% to prevent overexposure. This led to sharp channels with measured widths and depths of 45μm and 50μm, repectively.

2D Tesla valves have been investigated by researchers for microfluidic applications due to their fixed or no-moving-parts (NMP) valves [5, 6]. Habhab et. al. 3D printed Tesla valves with channels of 500 x 500 μm^2 in cross-sections but noted that further miniaturization of these channels is necessary for valvular conduits to be widely adopted in lab-on-a-chip applications [5]. The structure presented here has channels that are 10 times smaller compared to that of Habhab et. al. and serves as an example that microscale additive manufacturing can play an important role in the miniaturization of microfluidic devices. Another and perhaps more common technique of fabricating microfluidic devices is lithography based. It involves multiple steps such as patterning a substrate using photoresists, lithography, and etching. The patterned substrates then serve as negative molds to build devices out of PDMS. Forster et.al. [6] used this method to fabricate 2D Tesla Valves with 150 x 150 μm^2 channels, which are 3 times larger than the ones presented here. This implies that microscale additive manufacturing is comparable to lithography-based methods in terms of resolution and minimum feature size. The presented structure serves as an example that microscale additive manufacturing can either print microfluidic devices in a single step or be utilized for molding PDMS-based devices. However, there may be additional considerations for molding that are not presented here and need to be researched.

3.2 Microlumen Array

A microlumen array (Fig. 3) was another structure that has applications in microfluidics in template-assisted self-assembly (TASA). A template containing 4,096 lumens was fabricated, under 2 hours, at 10% laser power, 3 mm/s laser velocity, and 90% overlap. Like the previous print, a low laser velocity and high pitch were utilized so that the negative spaces can be printed with high resolution and precision. The entire part, excluding the base, were printed in a single slice to minimize the tapering commonly seen in resin 3D printing. As can be seen in Figure 3C, this phenomenon was not completely prevented, but its effect was minimized. The average diameter of the lumens was 12 μm at the top, reduced to 7 μm towards the center, and finished as 5 μm at the bottom. The lumens also have an average depth of 34(z) μm and are separated from edge-to-edge by 12(y) μm and 16(x) μm along and perpendicular to the writing direction, respectively. The discrepancy between these two separations was due to the fact that the lumens' two sides that were tangent to writing direction could not be completely printed, an inherent limitation of vat photopolymerization. As the laser approached the line tangent to the lumen, its timing was

too slow, therefore resulting in over-polymerization of the lumen edge. This also helps explain why the lumens were not perfectly circular but instead slightly elongated along the writing direction. This phenomenon was minimized using a very high pitch and low laser velocity; it would have been more emphasized if the pitch was lower, and the laser velocity was higher.

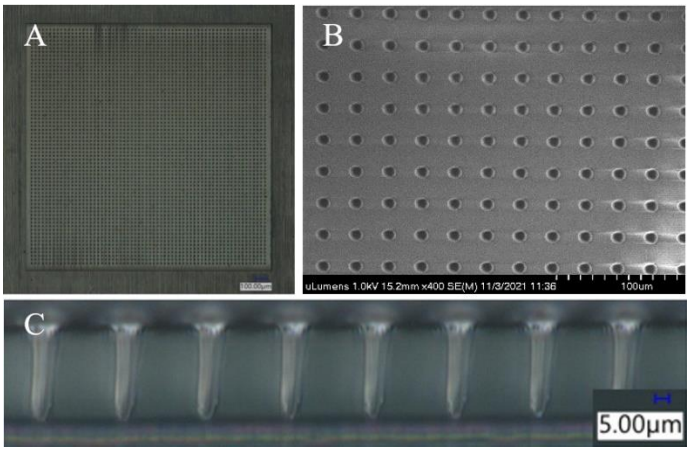

FIGURE 3: A: Digital light micrograph of the microlumen array at 40X magnification. B: Scanning electron micrograph of a section of the array at 400X magnification. C: Digital light micrograph showing the side views of the lumens that are penetrating down. As can be seen, the lumens are flat for the most part but taper down towards the bottom.

Physical templates such as the one presented here can assist monodispersed spherical colloids to assemble into aggregates with controlled size and form [7]. TASA structures are primarily used to research the hydrodynamic and optical scattering properties of colloidal particles [7] but can also be utilized for microfluidic applications for cell sorting, organization, and testing purposes. Yin et. al. [7] presented a series of patterned templates, each having a different confinement geometry such as lumens, triangles, squares, and columns and demonstrated the efficacy of such structures in assembling colloids. They fabricated these patterned arrays in thin films of photoresists through spin-coating and photolithography, achieving negative spaces ranging from 1µm to 5µm. The fabrication process outlined here is not capable of achieving features down to 1µm but has its own advantages such as it is a single step process that requires less manufacturing time.

3.3 Microneedle Array

Microneedle arrays are becoming increasingly important for drug delivery and biopharmaceutical purposes. Presented here is an array of 25 microneedles (Fig. 4) with base diameters and heights of 200µm and 650µm, respectively. They were fabricated with z-slicing at 10µm/layer, 10% laser power, 3mm/s laser velocity, and 90% pitch overlap. After the printing, the sample was developed in three subsequent IPA baths of 3 minutes each to wash away the uncured resin. It was dried with nitrogen gun after each IPA bath and finally post-cured under UV light for 7 minutes. Like previous structures, a low writing speed and high pitch were employed so that fine features can be printed with high resolution. The slice thickness could be reduced from 10µm/layer to 5µm/layer to further increase the z-resolution but at the expanse of printing time. The fabrication time was around 14 hours and the reduction in slice thickness would have doubled it. The needles had dimensions very close to that of designed: their bases, heights, and separations were measured to be around 203µm, 645µm, and 295µm, respectively. Additionally, the tips of the needles were measured to be around 6.5µm which is very close to the theoretical limit of the 3D printer, made possible by highly optimized process parameters. On the other hand, the tips were slightly bent towards the same direction, probably due to their lack of mechanical strength and stability. This preferential tilting might have been induced during the washing or drying procedure, before it obtained its final mechanical properties enabled by post-curing.

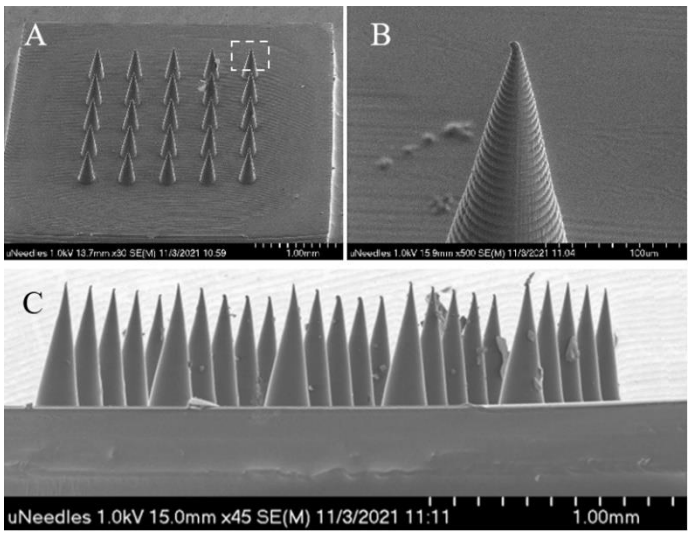

FIGURE 4: A: Scanning electron micrograph of the microneedle array. B: Scanning electron micrograph close-up on the tip of the microneedle framed in A; each indicial circular slice can be identified. C: Side view of the microneedle array. There are some impurities on the needles that probably occurred after the printing process.

Microneedles have several advantages such as robust immune response, greater longevity, and improved systematic drug absorption [8, 9] . Additionally, they are minimally invasive and can be painlessly self-administered. Common fabrication methods include etching [10], laser-cutting [11], and micromolding [9]. These techniques can manufacture high quality needles with tip diameters around 2-5µm but are usually expensive, time consuming and limited in design. The microneedles presented here have tip diameters comparable to that of conventional methods and fabricated in a single step. Additionally, additive manufacturing allows these structures to be designed with greater freedom and iterated with minimal

process development. There are examples of 3D printed microneedles in literature [12, 13], but these structures generally have tip diameters that are generally an order of magnitude larger than the ones presented here, limiting their wide adoption in drug delivery systems. Further research is needed to explore how various chemicals such as vaccines or drugs can be introduced onto the presented structure, but repeated dip-coating is a promising option [14]. Alternatively, this structure could serve as a mold such that a more conventional method of micromolding could be used to fabricate functionalized microneedle arrays.

3.4 Cubic fluorite microlattice

Lastly, a cubic fluorite microlattice (Fig. 5) was printed to demonstrate that microscale porous cellular architectures and overhangs can also be fabricated via micro vat photopolymerization. The microlattice was z-sliced at 20 μm/layer and fabricated at 40% laser power, 60 mm/s, and 50% overlap. The combination of all these build parameters resulted in a relatively low dose that prevented overexposure of the overhangs and kept the cells open. After 7.5 hours of printing, the structure was washed in two subsequent IPA baths of 12 minutes each and dried with nitrogen following each bath. Finally, the structure was post-cured in UV light for 5 minutes. The slight anisotropic shrinkage of the part was due to a combination of exposure and dehydration caused by the IPA bath. A low dose cured the resin less aggressively, leading to a cured structure with relatively low cross-link density. This in return caused the structure to strain more for a given force induced by the dehydration. The shrinkage was anisotropic because during the IPA bath the higher levels of the structure were not constrained and free to shrink while the base was still attached to the build platform which restrained the shrinkage of lower levels. The shrinkage could be forced to be isotropic by performing the IPA bath after removing the base from the substrate holder, rendering this phenomenon as a useful tool to obtain structures that are smaller than the ones designed and printed. For example, the printed struts and perforations have dimensions of 50 μm and 80 μm, respectively, which are both smaller than what was designed.

In the biomedical sector, architected cellular materials are important because they can be designed to mimic biological geometries, and hence act as bioscaffolds, with applications ranging from tissue engineering to regenerative medicine [1, 15]. For instance, Islam et. al. [15] presented a 3D printed carbon/fiber microlattice with an architecture similar to the one reported here and demonstrated its capability in culturing osteoblast-like cells for tissue repair applications. These cells can not only proliferate on the microlattice but can also make connections thanks to the porous scaffold. The presented microlattice serves as an example that micrometer sized structures with interconnected pores can be additively manufactured, and its architecture can be tailored to suit various engineering purposes. The fabrication process outlined here has the potential to scale down the microlattice, but further research is needed to investigate how the miniaturization of these structures can broaden their applications and uses.

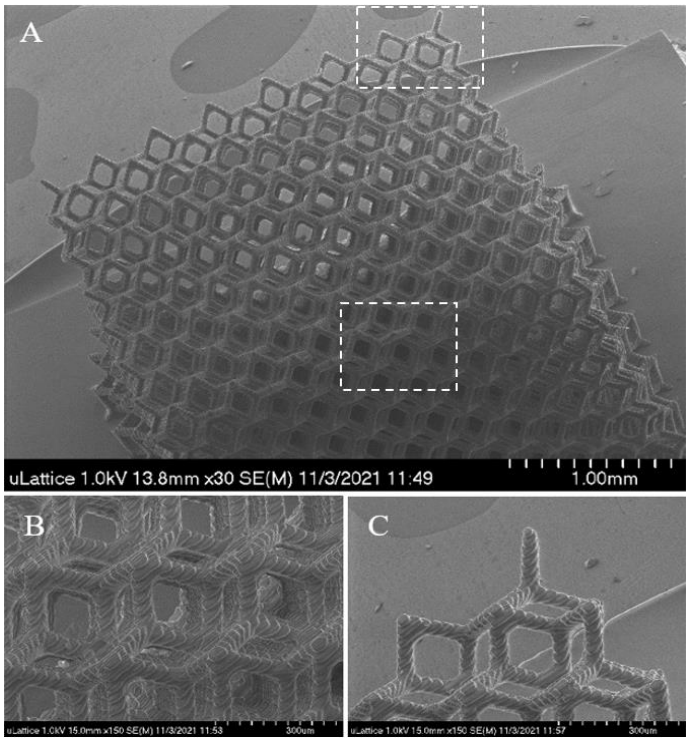

FIGURE 5: A: Scanning electron micrograph of the cubic fluorite microlattice; each individual unit cell with struts and perforations can be clearly identified. Close-up on the center (B) and corner (C) of the microlattice.

4. CONCLUSION

In this paper, the capability and fidelity of micro vat photopolymerization in fabricating microscale medical devices was demonstrated. For microfluidic applications, a 2D Tesla valve with a channel of 45(x) x 50(z) μm^2 cross-section, and a microlumen array consisting of 4,096 identical lumens with diameters, heights, and edge-to-edge separations of 12(x and y), 34(z), and 16(x) and 12(y) μm, respectively, were 3D printed. Additionally, a microneedle array containing conical shapes with minimum features as fine as 6.5 μm was fabricated as an example drug delivery system. Lastly, a cubic fluorite microlattice with struts and perforation as small as 50 μm and 80 μm, respectively, was produced to demonstrate the micro-additive manufacturing's potential in developing mesoscale architected materials that can act as bioscaffolds. These results serve as examples that micro vat photopolymerization is a feasible option to print microscale medical devices with qualities rivaling those manufactured via conventional methods. Further research is recommended to functionalize these structures.

ACKNOWLEDGEMENT

The authors acknowledge the Mayo Clinic Microscopy and Cell Analysis Core for support with SEM imaging.

REFERENCES

[1] Ngo, T. D., Kashani, A., Imbalzano, G., Nguyen, K. T. Q., and Hui, D., 2018, "Additive manufacturing (3D printing): A review of materials, methods, applications and challenges," Compos Part B-Eng, 143, pp. 172-196.
[2] Ahangar, P., Cooke, M. E., Weber, M. H., and Rosenzweig, D. H., 2019, "Current Biomedical Applications of 3D Printing and Additive Manufacturing," Appl Sci-Basel, 9(8).
[3] Voldman, J., Gray, M. L., and Schmidt, M. A., 1999, "Microfabrication in biology and medicine," Annu Rev Biomed Eng, 1, pp. 401-425.
[4] Dizon, J. R. C., Gache, C. C. L., Cascolan, H. M. S., Cancino, L. T., and Advincula, R. C., 2021, "Post-Processing of 3D-Printed Polymers," Technologies, 9(3).
[5] Habhab, M. B., Ismail, T., and Lo, J. F., 2016, "A Laminar Flow-Based Microfluidic Tesla Pump via Lithography Enabled 3D Printing," Sensors-Basel, 16(11).
[6] Foster, F. K., Bardell, R. L., Afromowitz, M. A., Sharma, N. R., and Blanchard, A., 1995, "Design, fabrication and testing of fixed-valve micro-pumps," Proceedings of the ASME Fluids Engineering Division, 234.
[7] Yin, Y. D., Lu, Y., Gates, B., and Xia, Y. N., 2001, "Template-assisted self-assembly: A practical route to complex aggregates of monodispersed colloids with well-defined sizes, shapes, and structures," J Am Chem Soc, 123(36), pp. 8718-8729.
[8] Wermeling, D. P., Banks, S. L., Huclson, D. A., Gill, H. S., Glupta, J., Prausnitz, M. R., and Stinchcom, A. L., 2008, "Microneedles permit transdermal delivery of a skin-impermeant medication to humans," P Natl Acad Sci USA, 105(6), pp. 2058-2063.
[9] Rouphael, N. G., Paine, M., Mosley, R., Henry, S., McAllister, D. V., Kalluri, H., Pewin, W., et al, 2017, "The safety, immunogenicity, and acceptability of inactivated influenza vaccine delivered by microneedle patch (TIV-MNP 2015): a randomised, partly blinded, placebo-controlled, phase 1 trial," Lancet, 390(10095), pp. 649-658.
[10] Henry, S., McAllister, D. V., Allen, M. G., and Prausnitz, M. R., 1998, "Microfabricated microneedles: A novel approach to transdermal drug delivery," J Pharm Sci, 87(8), pp. 922-925.
[11] Martanto, W., Davis, S. P., Holiday, N. R., Wang, J., Gill, H. S., and Prausnitz, M. R., 2004, "Transdermal delivery of insulin using microneedles in vivo," Pharm Res-Dordr, 21(6), pp. 947-952.
[12] Pere, C. P. P., Economidou, S. N., Lall, G., Ziraud, C., Boateng, J. S., Alexander, B. D., Lamprou, D. A., and Douroumis, D., 2018, "3D printed microneedles for insulin skin delivery," Int J Pharmaceut, 544(2), pp. 425-432.
[13] Lu, Y. F., Mantha, S. N., Crowder, D. C., Chinchilla, S., Shah, K. N., Yun, Y. H., Wicker, R. B., and Choi, J. W., 2015, "Microstereolithography and characterization of poly(propylene fumarate)-based drug-loaded microneedle arrays," Biofabrication, 7(4).
[14] Vassilieva, E. V., Kalluri, H., McAllister, D., Taherbhai, M. T., Esser, E. S., Pewin, W. P., Pulit-Penaloza, J. A., Prausnitz, M. R., Compans, R. W., and Skountzou, I., 2015, "Improved immunogenicity of individual influenza vaccine components delivered with a novel dissolving microneedle patch stable at room temperature," Drug Deliv Transl Re, 5(4), pp. 360-371.
[15] Islam, M., Sadaf, A., Gomez, M. R., Mager, D., Korvink, J. G., and Lantada, A. D., 2021, "Carbon fiber/microlattice 3D hybrid architecture as multi-scale scaffold for tissue engineering," Mat Sci Eng C-Mater, 126.